

## Surface valence transition in SmS by alkali metal adsorption

Takuto Nakamura<sup>1,2,\*</sup>, Toru Nakaya,<sup>2</sup> Yoshiyuki Ohtsubo<sup>3,1,2</sup>, Hiroki Sugihara,<sup>2</sup> Kiyohisa Tanaka,<sup>4</sup> Ryu Yukawa,<sup>5</sup> Miho Kitamura,<sup>6</sup> Hiroshi Kumigashira<sup>7</sup>, Keiichiro Imura<sup>8,†</sup>, Hiroyuki S. Suzuki,<sup>9</sup> Noriaki K. Sato,<sup>8,10</sup> and Shin-ichi Kimura<sup>1,2,4,‡</sup>

<sup>1</sup>Graduate School of Frontier Biosciences, Osaka University, Suita 565-0871, Japan

<sup>2</sup>Department of Physics, Graduate School of Science, Osaka University, Toyonaka 560-0043, Japan

<sup>3</sup>National Institutes for Quantum Science and Technology, Sendai 980-8579, Japan

<sup>4</sup>Institute for Molecular Science, Okazaki 444-8585, Japan

<sup>5</sup>Graduate School of Engineering, Osaka University, Suita 565-0871, Japan


<sup>6</sup>Photon Factory, Institute of Materials Structure Science, High Energy Accelerator Research Organization (KEK), 1-1 Oho, Tsukuba 305-0801, Japan

<sup>7</sup>Institute of Multidisciplinary Research for Advanced Materials (IMRAM), Tohoku University, Sendai 980-8577, Japan

<sup>8</sup>Department of Physics, Nagoya University, Nagoya 464-8602, Japan

<sup>9</sup>Institute for Solid State Physics, The University of Tokyo, Kashiwa 277-8581, Japan

<sup>10</sup>Center for General Education, Aichi Institute of Technology, Toyota 470-0392, Japan

 (Received 30 May 2022; revised 13 December 2022; accepted 14 December 2022; published 5 January 2023)

The electronic structure changes of SmS surfaces under potassium (K) doping are elucidated using synchrotron-based core-level photoelectron spectroscopy and angle-resolved photoelectron spectroscopy (ARPES). The Sm core-level and ARPES spectra indicate that the Sm mean valence of the surface increased from the nearly divalent to trivalent states, with increasing K deposition. Carrier-induced valence transition (CIVT) from Sm<sup>2+</sup> to Sm<sup>3+</sup> exhibits a behavior opposite to that under conventional electron doping. Excess electrons from K atoms are transferred to S sites and the liberated electrons from Sm<sup>3+</sup> ions due to CIVT at the surface are trapped like local excitons around the Sm<sup>3+</sup> ions, which is inconsistent with the phase transition from the black insulator with Sm<sup>2+</sup> to the gold metal with Sm<sup>3+</sup> under pressure. This CIVT helps to clarify the pressure-induced black-to-golden phase transition in this material, which originates from the Mott transition of excitons.

DOI: [10.1103/PhysRevB.107.L041102](https://doi.org/10.1103/PhysRevB.107.L041102)

At the boundary between localized and itinerant electron systems in solids, such as strongly correlated electron systems, fluctuations in the degrees of freedom of the electrons are origins of a variety of physical properties, especially unconventional superconductivity and giant magnetoresistance. Among such systems, the physical properties of rare-earth compounds mainly originates from the hybridization between the conduction electrons and 4*f* electrons, namely *c-f* hybridization as well as the Kondo effect [1,2]. Then, clarifying the valence condition and change gives us an understanding of the origin of the physical properties [3–6]. Among many valence fluctuation materials with rare-earth ions, samarium monosulfide (SmS) is a typical material indicating a pressure-induced valence transition.

In SmS, the physical properties strongly depend on the valence of the Sm ions [7]. At ambient pressure, SmS acts as a black-colored semiconductor with an indirect band gap of about 0.1 eV (namely black phase) [8,9], where the Sm ions are almost divalent [10]. In the angle-resolved photoelectron

spectroscopy (ARPES) spectrum, the top of the Sm<sup>2+</sup> 4*f* multiplet are localized at the binding energy of about 0.5 eV from the Fermi level [11]. In the optical conductivity spectra, indirect and direct energy gaps have been observed at the photon energies of ~0.1 eV and ~0.5 eV, respectively [12], which have been assigned the optical transition from the top of the valence band at the  $\Gamma$  point to the bottom of the conduction band at the *X* point and to the saddle point at the  $\Gamma$  point, respectively [8]. With applying pressure above the critical pressure of 0.65 GPa, the sample changes to a golden-yellow-colored metallic behavior (namely golden phase) but with a narrow gap, which is similar to that of SmB<sub>6</sub> at ambient pressure [13]. Although this pressure-induced black insulator-to-golden metal phase transition (BGT) was discovered more than 50 years ago [7], the origin of this phase transition still remains under debate [14]. In the golden phase, the mean valence of Sm becomes nearly trivalent [10] and a large conduction band consisting of the Sm 5*d* band is expected to exist, which will be strongly hybridized with the Sm 4*f* states [15]. This could be confirmed by the optical conductivity measurement under pressures [12]. To understand the electronic structure in the golden phase, ARPES measurement should be performed under high pressure, but the experimental technique is still a challenging topic. Instead, the band structure in SmS with applied chemical pressure due to

\*nakamura.takuto.fbs@osaka-u.ac.jp

†Present address: National Institutes for Institute of Liberal Arts and Sciences, Nagoya University, Nagoya 464-8601, Japan.

‡kimura.shin-ichi.fbs@osaka-u.ac.jp

yttrium (Y) substitution has been reported with ARPES [16]. By the substitution, the Sm  $4f$  and  $5d$  bands approach the Fermi level and cross each other, which is consistent with the band deformation due to applying pressure. However, a possibility of a metallic conduction path by a carrier doping from Y ions was also suggested [17], i.e., it has not been clarified yet which is the essential origin—lattice compression or carrier doping. Recently, a phase transition like the pressure-induced one has been reported due to two different types of perturbations: light irradiation and current injection [18,19]. These perturbations are commonly expected to increase carriers, namely carrier-induced valence transition (CIVT), but the detailed electronic states with carrier doping have not been clarified yet.

Alkali metal adsorption on crystal surfaces is a widely used method to investigate the effects of carrier injection into materials [20,21]. Owing to the electron doping from the alkali metal to the sample, the sample surface becomes negatively doped; sometimes a band structure rigidly shifts to the higher binding energy side. The doping concentration can be precisely manipulated by controlling the total amount of deposition. This technique is occasionally combined with ARPES to observe the unoccupied electronic states [22–24] and is also employed to observe the negative electron affinity on semiconductor surfaces, owing to the formation of the surface electric double layer [25]. Therefore, through alkali metal adsorption, a well-defined, carrier-doped SmS surface can be realized. Such a surface would serve as a suitable candidate for investigating the carrier doping effect.

In this Letter, we have studied the change of the electronic structure by potassium (K) doping on a SmS surface by synchrotron-based ARPES and core-level photoelectron spectroscopies. With increasing the amount of the K deposition, the Sm mean valence at the surface was increased from nearly divalent to trivalent, which is the opposite behavior observed in many materials, i.e., the mean valence normally decreases due to electron donation from the adsorbed alkali metal to the surface. This CIVT gives us important information in terms of clarifying the pressure-induced BGT in this material.

High-quality single-crystalline SmS was grown using the vertical Bridgman method in a high-frequency induction furnace [9]. A clean SmS surface was obtained via cleaving *in situ* in an ultrahigh vacuum chamber at room temperature (RT). K atoms were evaporated with a well-degassed alkali metal dispenser (SAES-Getters) at RT. The adsorption of K atoms on the samples was examined using core-level photoelectron spectroscopy, as shown in Fig. S1 in the Supplemental Material [26] (see, also, Ref. [27] therein). The thickness of K atoms was evaluated by using quartz microbalance and calibrated by the intensity of the K  $3p$  and Sm  $4p$  core levels. In this work, one monolayer (ML) of the evaporated K atoms was defined as the atomic density of bulk SmS.

ARPES and core-level photoelectron spectroscopy measurements were performed at BL5U of UVSOR-III and BL-2A MUSASHI of Photon Factory, with photon energies ranging from 35 to 1500 eV with  $p$  polarization. The energy resolutions of the ARPES and core-level photoelectron spectroscopy were set to  $\sim 30$  and  $\sim 100$  meV, respectively. The energy resolution and position of the Fermi level were

calibrated using the Fermi edge of the evaporated Au film. All the measurements were performed at RT.

Figures 1(a)–1(d) show the core-level spectra of Sm  $3d$  and  $4d$  as a function of the K deposition thickness. From Fig. 1(a), the Sm trivalent ( $\text{Sm}^{3+}$ ) and divalent ( $\text{Sm}^{2+}$ ) multiplet peaks are observed at kinetic energies of  $\sim 58$  and  $\sim 68$  eV, respectively. For 0-ML deposition (pristine SmS), the intensity of the  $\text{Sm}^{2+}$  peak was higher than that of the  $\text{Sm}^{3+}$  peak, suggesting that the Sm ions were nearly divalent. With increasing K deposition thickness, the  $\text{Sm}^{3+}$  component gradually became dominant. After the deposition of more than 5 ML, the core-level spectral shape remained unchanged, suggesting the saturation of the K adsorption. Since the substrate temperature was kept at RT through the whole experiment, the adsorption would be limited to a few monolayers, similar to that of other alkali metal adsorbed on semiconductor systems such as Cs/Si(001) surface [28].

As shown in Figs. 1(b)–1(d), the  $\text{Sm}^{3+}$  components became dominant with an increase in the K deposition thickness, similar to the results shown in Fig. 1(a). However, the rate of increase decreased as the kinetic energy of the photoelectrons increased. These results can be explained by the kinetic energy dependence of the effective traveling length of photoelectrons, as illustrated in Fig. 1(e). In the present case, the Sm  $3d$  and  $4d$  core levels excited by 1150 eV [Fig. 1(a)] and 1500 eV [Fig. 1(d)] photons are expected to be the most surface and bulk sensitive, respectively.

To obtain further information regarding the change in the Sm mean valence due to the K adsorption, the mean valence was evaluated from the peak area ratio between the  $\text{Sm}^{2+}$  and  $\text{Sm}^{3+}$  components in the core-level spectrum after subtracting the Shirley-type background, as shown in Fig. 1(f). With reference to the typical relationship between the kinetic energy and the inelastic mean free path of photoelectrons [29], the mean valences as a function of the photoelectron mean free path were obtained, as indicated by the marks in Fig. 1(g). The best fit and the obtained surface and bulk mean valences, determined via fitting with the formula in Supplemental Material 3, are presented as dashed lines in Fig. 1(g). (Another evaluation method for the depth dependence of the Sm mean valence is shown in S5 of the Supplemental Material. The obtained mean valences of the surface and bulk states evaluated by the method are almost consistent with that by our method.) Using these fitting parameters, the mean valences on the surface and in the bulk as a function of the K deposition thickness can be evaluated, as shown in Fig. 1(h). In pristine SmS, the mean valence at the surface was slightly closer to the divalent state than that of the bulk, as is generally observed in valence fluctuation materials [30], because of the lattice expansion at the surface. The mean valence of the surface component increased with the K deposition thickness below 2 ML. This behavior, however, is not typical because alkali metal adsorption is usually effective for electron doping. The maximum value of the surface mean valence was approximately 3.0, which is almost identical to that of the golden phase of SmS under high pressures. By contrast, in the bulk region, the mean value changed slightly from  $2.4 \pm 0.1$  to  $2.1 \pm 0.15$  with the increasing K content. These results suggest that the mean valence of the Sm ions on the SmS surface can be easily increased via electron doping, even though the bulk valence

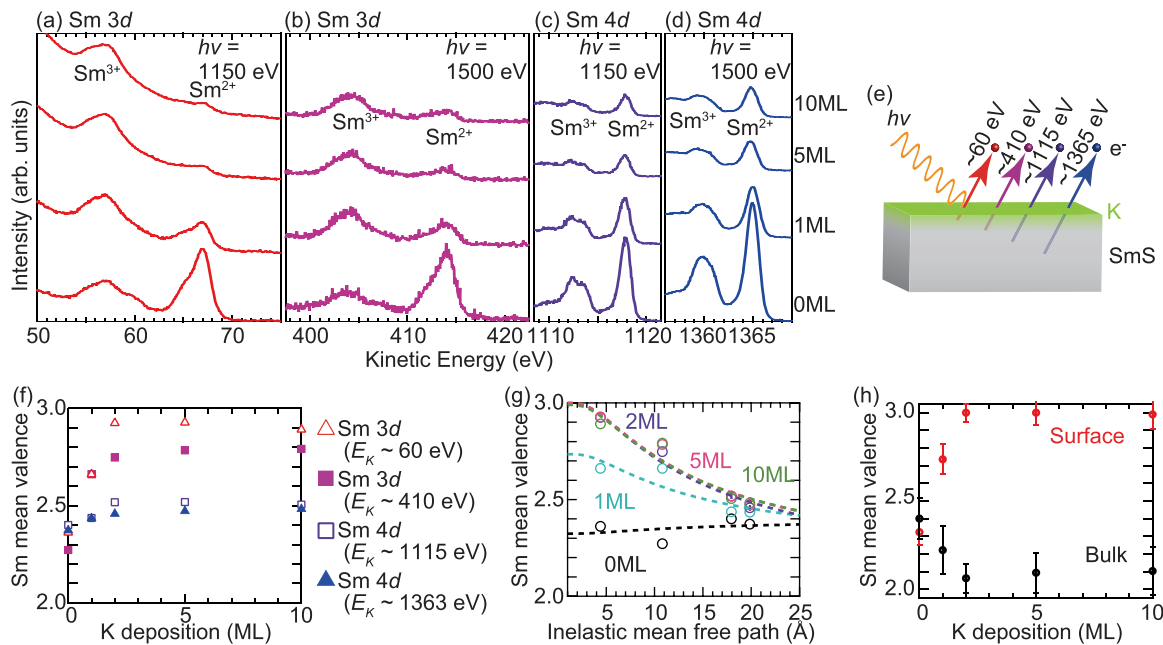


FIG. 1. (a),(b) Sm 3*d* and (c),(d) Sm 4*d* core-level spectra of SmS single crystals as a function of the amount of K deposition, with excitation photon energies at (a),(c) 1150 eV and (b),(d) 1500 eV. (e) Schematic of the photoemission detection depth for different kinetic energies. (f) Sm mean valence depending on K deposition, evaluated from the peak area ratio between the Sm<sup>3+</sup> and Sm<sup>2+</sup> multiplets after subtracting the Shirley-type background. (g) Sm mean valence as a function of the mean free path of photoelectrons. Dashed lines indicate the fitting curves expected with a two-layer model, shown in Supplemental Material S3. (h) Surface and bulk Sm mean valences as a function of the amount of K deposition, evaluated with the two-layer model.

is conserved. It should be noted that the absorption spectrum at the Sm *L* edge suggests that the bulk mean valence of Sm at ambient pressure is approximately Sm<sup>2+</sup> [10], which is inconsistent with our data. This discrepancy can be due to different probing depth in different methods.

The change of the mean valence is expected to be strongly influenced in the valence band ARPES spectra. The ARPES spectra of K-adsorbed SmS (K/SmS), as compared with those of pristine SmS, are shown in Fig. 2. The bulk Brillouin zone (BZ) of SmS is shown in Fig. 2(a). To identify the  $\Gamma$  point along the surface normal ( $k_z$ ) wave number, the excitation photon-energy dependence of the valence band spectrum at  $k_x = k_y = 0 \text{ \AA}^{-1}$  was measured, as shown in Fig. 2(b). The multiplet structure of the flat Sm<sup>2+</sup> 4*f*<sup>6</sup> final states and dispersive S 3*p* bands were observed near  $\sim 1.5$  and  $\sim 4.5$  eV, respectively. Note that the measured photoelectron spectra do not directly reflect the ground state of the SmS. In strongly electron correlated materials, the  $n - 1$  electron system, which is the  $n$  electron system minus one electron by photoexcitation, is observed as a photoelectron spectrum. By setting the inner potential to 14.1 eV from the folded period of the S 3*p* band, which is identical to that previously evaluated [16],  $h\nu \sim 60$  eV and  $\sim 95$  eV correspond to the  $\Gamma$  and *X* points along the  $k_z$  direction, respectively. Figure 2(c) shows the ARPES intensity plot of the pristine SmS along  $\Gamma$ -*X*, as obtained with 60-eV photons. As well as the  $k_z$  direction shown in Fig. 2(b), a flat Sm<sup>2+</sup> 4*f*<sup>6</sup> multiplet structure and dispersive S 3*p* bands were observed. The second-derivative ARPES image, highlighting the shape of the band dispersion, is shown in Fig. 2(d). The 4*f*<sup>6</sup> multiplets can be decomposed into three

components that are weakly dispersed from the  $\Gamma$  point to the *X* point. At binding energy of  $\sim 4$  eV, the well-dispersive three bands originated from S 3*p* and the discrete flat band is Sm 4*f*<sup>6</sup> *P* multiplets [11]. Figures 2(e) and 2(f) present ARPES images and a second-derivative plot, respectively, of the K/SmS surface with the K adsorption of 0.4 ML. On many alkali metal-adsorbed surfaces, electron doping causes a band shift toward the side with high binding energy; however, no such change was observed in this case. This result suggests that the change of the electronic structure of the K/SmS surface cannot be explained by a simple rigid band shift model due to electron doping.

To obtain further insights into the deformation of the band structure owing to K adsorption, magnified images of the second-derivative ARPES for the 4*f* bands are shown in Figs. 3(a) and 3(b). In pristine SmS, the three branches located at 1, 1.7, and 2.5 eV in the 4*f* bands observed in ARPES are assigned to the multiplets of bulk-<sup>6</sup>*H*, sum of bulk-<sup>6</sup>*F* and surface-<sup>6</sup>*H*, and surface-<sup>6</sup>*F*, respectively. Figure 3(c) and 3(d) show the energy distribution curves at the  $\Gamma$  and *X* points of the pristine-SmS and K/SmS surfaces, respectively. To clarify the contributions of the surface and bulk components, the peaks were separated by Gaussian fittings. After the K deposition, the surface components were suppressed; this is consistent with the behavior of the core-level peaks in Fig. 1.

The core-level photoelectron spectra and ARPES results commonly suggest that CIVT from Sm<sup>2+</sup> to Sm<sup>3+</sup> occurs on the SmS surface; however, this cannot be explained from the perspective of a simple rigid band picture. We now discuss the role of the excess electrons generated by the change from

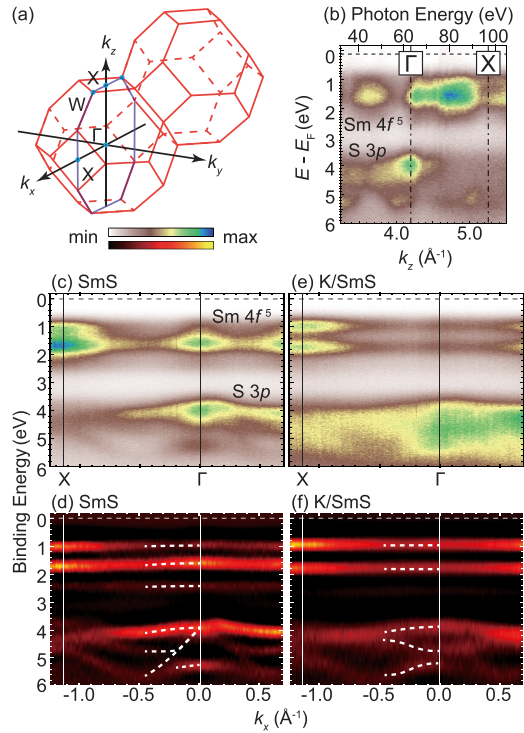


FIG. 2. (a) Three-dimensional bulk Brillouin zone of SmS. (b) Photon-energy dependence of valence band spectra at normal emission ( $k_x = k_y = 0 \text{ \AA}^{-1}$ ). Intensities of the photoelectron are normalized by maximum counts of the valence band spectra at each excitation energy in the measured energy range (binding energy = 0–6.0 eV). Inner potential was set to 14.1 eV, based on the periodicity of the S 3*p* band around 4.5 eV. (c) ARPES intensity plot and (d) second derivative of the ARPES intensity of the pristine-SmS surface along  $\Gamma$ -X, with 60 eV photons ( $k_z \sim 0 \text{ \AA}^{-1}$ ), respectively. (e), (f) Same as (c), (d) but for the K-adsorbed SmS (K/SmS) surface. White dashed lines serve as guides for the band dispersion.

Sm<sup>2+</sup> to Sm<sup>3+</sup>. In the pressure-induced golden phase attained via BGT, the excess electrons became conduction electrons. However, the overall electronic state near the Fermi level retains a semiconducting nature, without any change caused by the K adsorption, as shown in Figs. 4(a) and 4(b). In other words, the surface electronic state did not become metallic under K doping. On the other hand, as shown in Figs. 4(c) and 4(d), the S 2*p* core-level peak is a single component in pristine SmS, with only two peaks separated by spin-orbit interaction (SOI), while in K/SmS, a new SOI-separated peak appears at the low energy side of the double peak observed in pristine SmS. The S ion in pristine SmS had a single valence number (S<sup>2-</sup>), whereas that in K/SmS featured two types of valences, suggesting the appearance of S<sup>2- $\delta$</sup>  ions, corresponding to the transfer of the excess electrons from K atoms to S sites. Considering that K/SmS remained in the semiconducting state and the Sm valence of the surface was trivalent, the excess electrons generated by the appearance of Sm<sup>3+</sup> can be regarded as being trapped like local excitons [the top figures of Fig. 4(e)] to conserve the charge neutrality. These results suggest that the liberated electrons due to CIVT at the surface are trapped like local excitons around the Sm<sup>3+</sup> ions, which is inconsistent with the phase transition from the

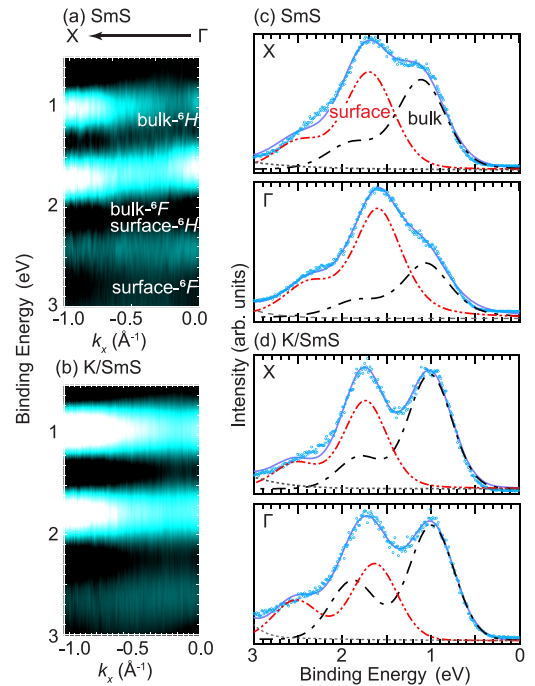


FIG. 3. (a), (b) Second derivative of ARPES intensity maps near the Fermi level along  $\Gamma$ -X, with 60 eV photons of (pristine) SmS and 0.4 ML-K/SmS. <sup>6</sup>H and <sup>6</sup>F indicate the multiplet structures of the Sm 4*f*<sup>5</sup> final state after photoexcitation. (c) Energy distribution curves (EDCs) at the  $\Gamma$  point (lower panel) and the X point (upper panel) of the SmS surface with the fitting curves. Dots and lines represent the raw data and fitted spectra (dash-dotted line: bulk component; dash-double-dotted line: surface component; solid line: sum of the bulk and surface components). Each component is fitted by the Voigt function after subtracting the Shirley-type background (dashed line). (d) Same as (c) but for the 0.4 ML-K/SmS surface.

black insulator with Sm<sup>2+</sup> to the gold metal with Sm<sup>3+</sup> under pressure.

These results were compared with the electronic state of the gold metallic phase under pressure. When pressure is applied, the lattice parameter decreases by approximately 5% owing to the decrease in the ionic radius of Sm by the BGT [10] and a carrier density similar to that of a monovalent metal is developed. (This is the origin of the golden color.) However, in the case of K/SmS, the bulk electronic state remained unchanged, suggesting that the bulk lattice constant was almost unchanged. Because the surface lattice constant does not differ significantly from the bulk lattice constant, it was considered to be almost unchanged. Under these conditions, conduction electrons do not appear, even if the Sm ions on the surface become trivalent, suggesting that the conduction electrons in the pressure-induced golden phase originate from the decrease in the lattice constant. Thus the origin of these conduction electrons in the golden phase is attributed to the decrease in the lattice parameter.

K doping to SmS induces the charge transfer from Sm to S atoms at the surface, which is a local event, like localized excitons produced by the photoexcitation from the Sm 4*f* to 5*d* orbitals. This phenomenon is considered to be similar to those for the insulator-to-metal transition caused by the

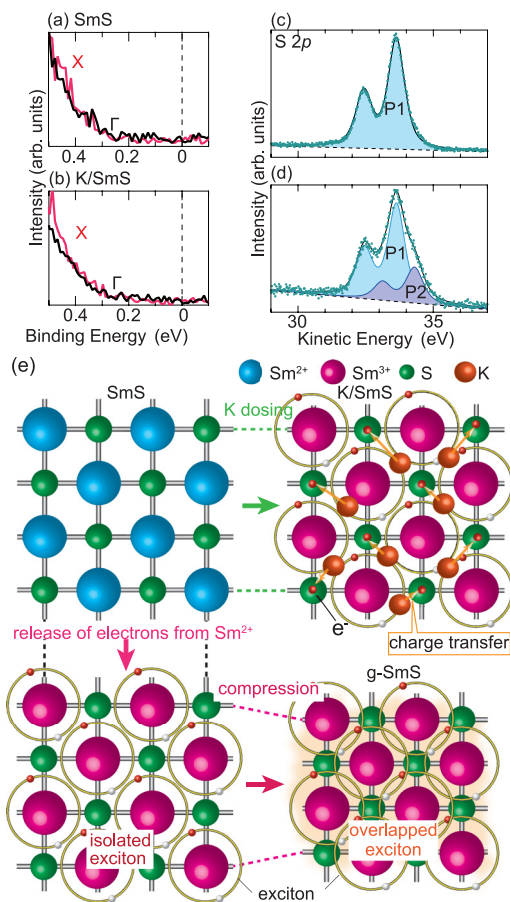


FIG. 4. (a) EDCs at the  $\Gamma$  point (black line) and  $X$  point (green line) of pristine SmS with 200 eV photons. (b) Same as (a) but for 0.4 ML-K/SmS. S  $2p$  core-level spectra of (c) pristine SmS and (d) K/SmS with 200-eV photons. Dashed lines indicate the Shirley-type background. Blue dots and black lines represent the raw data and fitted curve using the Voigt function and background. (e) Schematic of the phase transition of SmS. Top left and top right images depict the real space image of pristine SmS and K/SmS, respectively. The large (small) sphere indicates the Sm (S) ion. The bottom left figure is an expected model of electron-doped SmS, while retaining the same lattice constant as pristine SmS, in contrast to the golden phase of SmS, by applying pressure, as shown in the bottom right figure. Yellow circles depict the electron-hole pairs (excitons).

Mott transition of excitons [31]. According to the recent theoretical study [14], both the first order valence transition and semimetal-semiconductor transition occur at the same time by the Coulomb repulsion between Sm  $4f$  and  $5d$  orbitals and exciton is condensate in both the black insulator and golden semimetallic phase. If the critical distance of the Mott transition of an exciton represents the lattice constant at the critical pressure of the BGT, then the BEC-BCS phase transition of the exciton occurs when the exciton size exceeds the critical lattice constant, as shown in the lower figures of Fig. 4(e). In the case of a change in the surface valence alone, there are no variations in the lattice constant; hence, even if electrons are released from the Sm ions, they are trapped by the isolated excitons. Therefore, the phase remains in the BEC state, which is consistent with the fact that no metal-insulator transition appears. The exciton Mott transition has been experimentally proposed in the photoexcited semiconductor systems [32–34]; however, the formation of such a state without optical excitation has never been reported to the best of our knowledge. This result strongly suggests that the CIVT is not directly linked with the insulator-metal transition and may provide useful information regarding the origin of the pressure-induced BGT.

In conclusion, we have studied the electronic structure on K adsorbed SmS surface by using synchrotron-based core-level photoelectron spectroscopies and ARPES. With an increase in the amount of K deposition, the mean valence of Sm at the surface increased from the nearly divalent to trivalent states, without a rigid band shift. This result suggests that the injected carriers induce the valence transition of the Sm ions from  $\text{Sm}^{2+}$  to  $\text{Sm}^{3+}$ , which is opposite to the charge transition observed under trivial electron doping, without an insulator-metal transition observed in the pressure-induced phase transition. The lack of metallization is considered to originate from the carriers being trapped by isolated excitons.

We thank T. Ito and H. Watanabe for helpful discussions. The ARPES and core-level PES measurements were performed under the UVSOR proposals (No. 21-666 and No. 21-855) and Photon Factory proposal (No. 2019G514). This study was supported by JSPS KAKENHI (Grants No. JP20K03859, No. JP19H01830, No. JP20H04453, and No. JP21H01028) and the Murata Science Foundation.

- [1] P. Gegenwart, Q. Si, and F. Steglich, *Nat. Phys.* **4**, 186 (2008).
- [2] C. Pfleiderer, *Rev. Mod. Phys.* **81**, 1551 (2009).
- [3] J. M. Lawrence, P. S. Riseborough, and R. D. Parks, *Rep. Prog. Phys.* **44**, 1 (1981).
- [4] I. Felner and I. Nowik, *Phys. Rev. B* **33**, 617 (1986).
- [5] I. Felner, I. Nowik, D. Vaknin, Ulrike Potzel, J. Moser, G. M. Kalvius, G. Wortmann, G. Schmiester, G. Hilscher, E. Gratz, C. Schmitzer, N. Pillmayr, K. G. Prasad, H. de Waard, and H. Pinto, *Phys. Rev. B* **35**, 6956 (1987).
- [6] K. Miyake and S. Watanabe, *J. Phys. Soc. Jpn.* **83**, 061006 (2014).
- [7] A. Jayaraman, V. Narayanamurti, E. Bucher, and R. G. Maines, *Phys. Rev. Lett.* **25**, 1430 (1970).
- [8] S. Kimura, T. Mizuno, K. Matsubayashi, K. Imura, H. S. Suzuki, and N. K. Sato, *Phys. B: Condens. Matter* **403**, 805 (2008).
- [9] K. Matsubayashi, K. Imura, H. S. Suzuki, T. Mizuno, S. Kimura, T. Nishioka, K. Kodama, and N. K. Sato, *J. Phys. Soc. Jpn.* **76**, 064601 (2007).
- [10] K. Imura, Y. Suzuki, N. Kawade, K. Sakamoto, K. Deguchi, H. Yamaoka, Y. Yamamoto, J. Mizuki, N. Hiraoka, H. Ishii, H. S. Suzuki, and N. K. Sato, *JPS Conf. Proc.* **30**, 011131 (2020).

- [11] T. Ito, A. Chainani, H. Kumigashira, T. Takahashi, and N. K. Sato, *Phys. Rev. B* **65**, 155202 (2002).
- [12] T. Mizuno, T. Iizuka, S. Kimura, K. Matsubayashi, K. Imura, H. S. Suzuki, and N. K. Sato, *J. Phys. Soc. Jpn.* **77**, 113704 (2008).
- [13] K. Matsubayashi, K. Imura, H. S. Suzuki, G. Chen, N. Mori, T. Nishioka, K. Deguchi, and N. K. Sato, *J. Phys. Soc. Jpn.* **76**, 033602 (2007).
- [14] S. Watanabe, *J. Phys. Soc. Jpn.* **90**, 023706 (2021).
- [15] V. N. Antonov, B. N. Harmon, and A. N. Yaresko, *Phys. Rev. B* **66**, 165208 (2002).
- [16] M. Kaneko, M. Saito, T. Ito, K. Imura, T. Hajiri, M. Matsunami, S. Kimura, H. S. Suzuki, and N. K. Sato, *JPS Conf. Proc.* **3**, 011080 (2014).
- [17] K. Imura, M. Saito, M. Kaneko, T. Ito, T. Hajiri, M. Matsunami, S. Kimura, K. Deguchi, H. S. Suzuki, and N. K. Sato, *J. Phys.: Conf. Ser.* **592**, 012028 (2015).
- [18] R. Kitagawa, H. Takebe, and K. Morinaga, *Appl. Phys. Lett.* **82**, 3641 (2003).
- [19] H. Ando, K. Sakamoto, K. Imura, K. Deguchi, H. S. Suzuki, and N. K. Sato, *JPS Conf. Proc.* **30**, 011132 (2020).
- [20] T. Aruga and Y. Murata, *Prog. Surf. Sci.* **31**, 61 (1989).
- [21] R. Diehl and R. McGrath, *J. Phys.: Condens. Matter* **9**, 951 (1997).
- [22] Z.-H. Zhu, G. Levy, B. Ludbrook, C. N. Veenstra, J. A. Rosen, R. Comin, D. Wong, P. Dosanjh, A. Ubaldini, P. Syers, N. P. Butch, J. Paglione, I. S. Elfimov, and A. Damascelli, *Phys. Rev. Lett.* **107**, 186405 (2011).
- [23] P. Zhang, P. Richard, N. Xu, Y.-M. Xu, J. Ma, T. Qian, A. V. Fedorov, J. D. Denlinger, G. D. Gu, and H. Ding, *Appl. Phys. Lett.* **105**, 172601 (2014).
- [24] R. Yukawa, M. Minohara, D. Shiga, M. Kitamura, T. Mitsuhashi, M. Kobayashi, K. Horiba, and H. Kumigashira, *Phys. Rev. B* **97**, 165428 (2018).
- [25] B. Goldstein, *Surf. Sci.* **35**, 227 (1973).
- [26] See Supplemental Material at <http://link.aps.org/supplemental/10.1103/PhysRevB.107.L041102> for the additional photoelectron spectroscopy data sets and detailed calculation method to the depth dependence of the Sm mean valence.
- [27] J. J. Yeh and I. Lindau, *At. Data Nucl. Data Tables* **32**, 1 (1985).
- [28] R. Holtom and P. M. Gundry, *Surf. Sci.* **63**, 263 (1977).
- [29] M. P. Seah and W. A. Dench, *Surf. Interface Anal.* **1**, 2 (1979).
- [30] K. Hagiwara, Y. Takeno, Y. Ohtsubo, R. Yukawa, M. Kobayashi, K. Horiba, H. Kumigashira, J. Rault, P. Le Fèvre, F. Bertran, A. Taleb-Ibrahimi, F. Iga, and S. Kimura, *J. Phys.: Conf. Ser.* **807**, 012003 (2017).
- [31] D. Guerci, M. Capone, and M. Fabrizio, *Phys. Rev. Mater.* **3**, 054605 (2019).
- [32] M. Dendzik, R. P. Xian, E. Perfetto, D. Sangalli, D. Kutnyakhov, S. Dong, S. Beaulieu, T. Pincelli, F. Pressacco, D. Curcio *et al.*, *Phys. Rev. Lett.* **125**, 096401 (2020).
- [33] E. Baldini, T. Palmieri, A. Dominguez, A. Rubio, and M. Chergui, *Phys. Rev. Lett.* **125**, 116403 (2020).
- [34] T. Siday, F. Sandner, S. Brem, M. Zizlsperger, R. Perea-Causin, F. Schiegl, S. Nerreter, M. Plankl, P. Merkl, F. Mooshammer, M. A. Huber, E. Malic, and R. Huber, *Nano Lett.* **22**, 2561 (2022).